Arch. Pharm. Chem. Life Sci. 2016, *349*, 1–14

ARCH PHARM
Archiv der Pharmazie

Full Paper

Characterization of the Fluorescence Properties of 4-Dialkylaminochalcones and Investigation of the Cytotoxic Mechanism of Chalcones

Bo Zhou[1], Peixin Jiang[2], Junxuan Lu[2], and Chengguo Xing[1]

[1] Department of Medicinal Chemistry, College of Pharmacy, University of Minnesota, Minneapolis, MN, USA
[2] Department of Biomedical Sciences, School of Pharmacy, Texas Tech University Health Sciences Center, Amarillo, TX, USA

Understanding the mechanisms responsible for the various biological activities of chalcones, particularly the direct cellular targets, presents an unmet challenge. Here, we prepared a series of fluorescent chalcone derivatives as chemical probes for their mechanistic investigation. Upon systematic physicochemical characterization, we explored their potential to elucidate the mode of action of chalcones' cytotoxicity. The fluorescence of the chalcones was found to be highly sensitive to structural and environmental factors. Structurally, a 4-dialkylamino group on the B ring, suitable electronic properties of the A ring substituents, and the planar conformation of the chalcone's core structure were essential for optimal fluorescence. Environmental factors influencing fluorescence included solvent polarity, pH, and the interactions of the chalcones with proteins and detergents. It was found that 18 chalcones showed a fluorescent brightness greater than 6000 $M^{-1} cm^{-1}$ in DMSO. However, water dramatically quenched the fluorescence, although it could be partially recovered in the presence of BSA or detergents. As expected, these fluorescent chalcones showed a sharp structure–activity relationship in their cellular cytotoxicity, leading to the identification of structurally similar cytotoxic and non-cytotoxic fluorescent chalcones as chemical probes. Confocal microscopy results revealed the co-localization of the cytotoxic probe **C8** and tubulin in cells, supporting tubulin as the direct cellular target responsible for the cytotoxicity of chalcones.

Keywords: Chalcone / Cytotoxicity / Fluorescent probe / Tubulin

Received: February 10, 2016; Revised: April 14, 2016; Accepted: April 22, 2016

DOI 10.1002/ardp.201500434

Additional supporting information may be found in the online version of this article at the publisher's web-site.

Introduction

Chalcones, or 1,3-diphenyl-2-propen-1-ones, are an important class of widely existing natural products with numerous synthetic analogs [1]. Various chalcones exhibit a wide spectrum of biological activities [2], including anti-cancer [3], anti-inflammatory [4], anti-microbial [5], anti-oxidant [6], and anti-diabetic [7] properties (Fig. 1). Many potential modes of actions and cellular targets have been proposed to account for these diverse bioactivities [8]. Detailed mechanisms, particularly the direct cellular targets responsible for these bioactivities, however, remain largely open. Cytotoxicity, for instance, a parameter indicative of chalcones' anti-cancer potential, has been extensively studied [9]. Sharp structure–activity relationships (SAR) have been observed, suggesting a well-defined interaction between chalcones and

Correspondence: Dr. Chengguo Xing, Department of Medicinal Chemistry, College of Pharmacy, University of Minnesota, 2231 6th St. SE, Minneapolis, MN 55455, USA.
E-mail: xingx009@umn.edu
Fax: +1-612-624-4996

ARCH PHARM
Archiv der Pharmazie

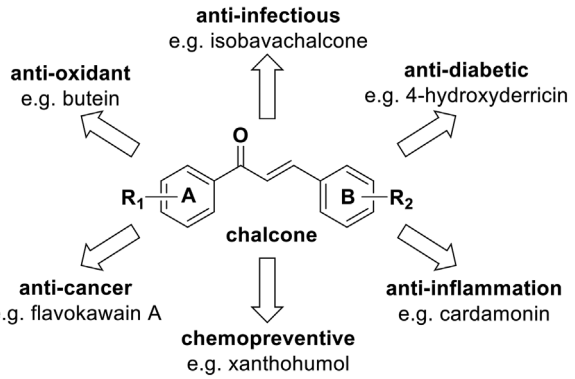

Figure 1. The core structure of chalcones and exemplary bioactivities.

the responsible cellular target for cytotoxicity [10, 11]. A number of putative targets have been proposed, including tubulin [12, 13], several kinases [14–16], cathepsins [17], topoisomerases [18], MDM2 [19], and many others [20–24]. However, data to date are far from sufficient to suggest any direct interactions of chalcones with these targets in cells. The lack of such knowledge greatly limits chalcones' selectivity improvement, efficacy optimization, and translational development.

Fluorescence-based approaches, such as fluorescence microscopy and fluorescence-based binding assays, either alone or in combination with other techniques, have been widely utilized to characterize small molecule-target direct interactions [25–28]. These approaches take advantage of the changes in fluorescence upon target binding [28]. To construct a fluorescent chemical probe, an extra fluorophore typically needs to be incorporated into the small molecule of interest, which has the potential disadvantage of interfering with target interaction. Chalcones with appropriate substituents have been reported to be intrinsically fluorescent, potentially avoiding such a disadvantage as fluorescent probes. For instance, Lee et al. [29] developed a library of fluorescent chalcones bearing 4-amido and 4-dialkylamino substitutions on the A and B rings, respectively; and one candidate selectively stained mouse embryonic stem cells, possibly through interacting with cell surface glycogens. Similarly, Ono et al. [30] discovered a 4-dialkylamino chalcone that fluorescently stained Aβ plaques in AD mice brains, and Tomasch et al. [31] developed fluorescent chalcones with extended double bonds as probes to target human histamine H3 receptor. However, such intrinsic fluorescence has not been explored to elucidate the mechanisms responsible for chalcones' diverse biological activities. Moreover, the effects of structural and environmental factors on chalcones' fluorescence, which are critical for their application as fluorescence-based chemical probes [28], have not been systematically characterized.

We herein constructed a library of chalcones, characterized the structural effects on their intrinsic fluorescence, evaluated the influence of several biologically relevant environmental factors, and investigated the potential of one lead as a chemical probe for cytotoxic target exploration.

Results and discussion

Design and synthesis of potentially fluorescent chalcones

One common feature of reported fluorescent chalcones is a dialkylamino substituent at the 4-position on the B ring (the phenyl ring to which the alkene is attached) [29–37]. Therefore, we designed our chalcone library mainly by fixing the dialkylamino group on the B ring and varying the substituents on the A ring (the phenyl ring to which the carbonyl is attached). Some related members, such as ring-constrained chalcones, chalcones with extended conjugation systems, and heterocyclic chalcones, have been designed as well. The syntheses of these compounds were accomplished through a conventional base-catalyzed aldol condensation reaction between the corresponding acetophenone-type and benzaldehyde-type analogs with appropriate substituents. Overall, we obtained 56 chalcones with diverse substituents and varied conjugation systems (Table 1).

Structural effects on fluorescence properties

Several optical properties of a fluorophore are critical for its potential application as a chemical probe [38]. The absorption and emission wavelengths determine the dynamic range of detection. The detecting sensitivity is largely dictated by the fluorescence brightness (B), which is the product of the extinction coefficient (ε) at the maximum absorption wavelength and the quantum yield (Φ) [39]. We therefore have characterized these optical properties of all 56 compounds in DMSO (Table 1, Fig. 2). Most compounds showed similar absorption. Their maximum absorption wavelengths are typically between 390 and 460 nm, with an extinction coefficient of 28000 to 38000 (Table 1, Fig. 2A and C). Their emission spectra, on the other hand, are much more sensitive to structural differences with large variations. The maximum emission wavelengths range from 450 to 620 nm (Table 1, Fig. 2B) and the quantum yields vary from 0 to 0.40 (Table 1, Fig. 2C). Eighteen compounds showed a fluorescent brightness of $>6000\,M^{-1}cm^{-1}$ (Table 1, Fig. 2D), comparable to fluorophores that have been successfully used in biological applications (e.g., Cy 3.18–$6000\,M^{-1}cm^{-1}$ and Atto 740–12000 $M^{-1}cm^{-1}$) [38]. These results overall suggest that a number of the synthesized chalcones are bright enough as potential fluorescent probes.

In addition, some structural effects on chalcones' fluorescence properties were observed (Fig. 3). First, an electron-donating dialkylamino group at the 4-position on the B ring is essential for fluorescence, because compounds lacking this

Table 1. **The structures, the cytotoxicity, and the optical properties of synthesized chalcones.**

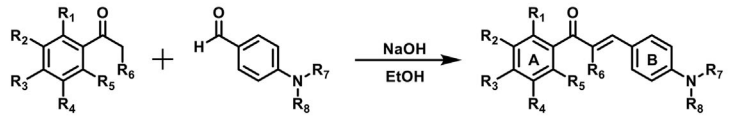

Cmpd.	R_1	R_2	R_3	R_4	R_5	R_6	R_7	R_8	IC_{50} (μM)	Abs λ_m (nm)	Emi λ_m (nm)	ε ($M^{-1}cm^{-1}$)	Φ
C1	H	H	H	H	H	H	–Me	–Me	23.2 ± 2.56	425	545	32400	0.24
C2	–OMe	H	H	H	H	H	–Me	–Me	0.25 ± 0.05	407	542	28000	0.23
C3	H	–OMe	H	H	H	H	–Me	–Me	2.00 ± 0.23	426	547	31500	0.23
C4	H	H	–OMe	H	H	H	–Me	–Me	>60	417	528	30700	0.38
C5	–OMe	H	–OMe	H	H	H	–Me	–Me	5.73 ± 0.49	409	529	30000	0.23
C6	–OMe	H	H	H	–OM	H	–Me	–Me	>60	394	488	33400	0.06
C7	H	–OMe	–OMe	H	H	H	–Me	–Me	17.02 ± 2.13	420	531	33000	0.40
C8	H	–OMe	H	–OMe	H	H	–Me	–Me	0.79 ± 0.22	427	548	31700	0.20
C9	H	–OMe	–OMe	–OMe	H	H	–Me	–Me	0.92 ± 0.18	425	540	33700	0.31
C10	–OMe	H	–OMe	H	–OM	H	–Me	–Me	>60	395	490	34800	0.02
C11	H	$-OCH_2O-$		H	H	H	–Me	–Me	8.89 ± 1.98	422	537	33500	0.38
C12	–OH	H	–OMe	H	–OM	H	–Me	–Me	>60	442	/[a]	34100	0
C13	–OH	H	H	H	H	H	–Me	–Me	>60	451	540	32800	0.01
C14	–Me	H	H	H	H	H	–Me	–Me	1.75 ± 0.07	407	528	31400	0.19
C15	H	H	–Me	H	H	H	–Me	–Me	>60	422	537	30700	0.36
C16	H	–Me	H	–Me	H	H	–Me	–Me	1.25 ± 0.14	422	539	30100	0.32
C17	H	H	$-CF_3$	H	H	H	–Me	–Me	>60	434	585	32200	0.02
C18	–F	H	–OEt	–F	H	H	–Me	–Me	>60	425	546	34100	0.11
C19	–F	H	–F	H	H	H	–Me	–Me	>60	420	548	36500	0.07
C20	H	H	–F	H	H	H	–Me	–Me	28.73 ± 11.67	430	543	32900	0.21
C21	H	H	–Cl	H	H	H	–Me	–Me	>60	431	558	34100	0.15
C22	H	H	–Br	H	H	H	–Me	–Me	>60	433	561	36000	0.14
C23	H	H	–I	H	H	H	–Me	–Me	31.89 ± 7.26	432	564	36300	0.14
C24	–Br	H	H	H	H	H	–Me	–Me	1.22 ± 0.04	409	545	37300	0.04
C25	$-NO_2$	H	H	H	H	H	–Me	–Me	3.34 ± 0.71	410	544	31300	<0.01
C26	H	$-NO_2$	H	H	H	H	–Me	–Me	>60	440	/[a]	34800	0
C27	H	H	$-NO_2$	H	H	H	–Me	–Me	>60	458	/[a]	24000	0
C28	H	H	$-NMe_2$	H	H	H	–Me	–Me	>60	422	521	45800	0.06
C29	H	H	–Ph	H	H	H	–Me	–Me	>60	430	566	29400	0.20
C30	H	H	H	H	H	–Me	–Me	–Me	0.43 ± 0.20	299	/[a]	10700	0
C31	H	H	–OMe	H	$-CH_2CH_2-$		–Me	–Me	>60	413	534	24800	0.02
C32	H	H	H	H	–C(=O)–		–Me	–Me	>60	493	549	67100	<0.01
C33	H	–OMe	–OMe	–OMe	H	H	–Et	–Et	0.35 ± 0.04	436	538	28500	0.40
C34	H	–OMe	–OMe	–OMe	H	H	–Me	$-(CH_2)_2OH$	0.31 ± 0.03	432	542	25500	0.36
C35	H	–OMe	–OMe	–OMe	H	H	$-(CH_2)_4-$		>60	435	543	31400	0.34
C36	H	–OMe	–OMe	–OMe	H	H	$-(CH_2)_5-$		19.01 ± 1.58	415	546	23600	0.33
C37	H	–OMe	–OMe	–OMe	H	H	$-(CH_2)_2O(CH_2)_2-$		0.73 ± 0.06	400	538	30500	0.38

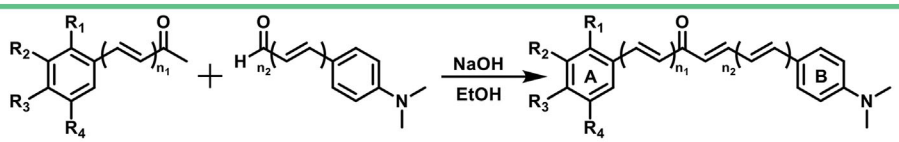

Cmpd.	R_1	R_2	R_3	R_4	n1	n2	IC_{50} (μM)	Abs λ_m (nm)	Emi λ_m (nm)	ε ($M^{-1}cm^{-1}$)	Φ
C38	–OMe	H	H	H	0	1	39.38 ± 6.48	431	603	29700	0.09
C39	H	–OMe	H	H	0	1	>60	446	616	30700	0.15
C40	H	–OMe	–OMe	–OMe	0	1	12.51 ± 1.55	447	610	32100	0.16
C41	H	–Me	H	–Me	0	1	3.09 ± 0.31	443	613	30900	0.14
C42	–Me	H	H	H	0	1	37.66 ± 11.33	432	585	28900	0.07
C43	–NO2	H	H	H	0	1	>60	438	/[a]	38900	0
C44	H	H	H	H	1	0	>60	427	611	31700	0.01

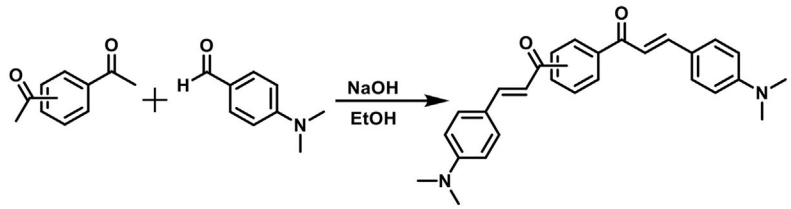

Cmpd.	Position of substitution	IC_{50} (μM)	Abs λ_m (nm)	Emi λ_m (nm)	ε ($M^{-1}cm^{-1}$)	Φ
C45	*Meta*–	>60	435	555	57900	<0.01
C46	*Para*–	>60	453	594	44300	<0.01

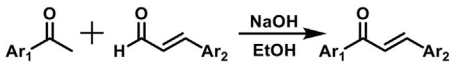

Cmpd.	Ar_1	Ar_2	IC_{50} (μM)	Abs λ_m (nm)	Emi λ_m (nm)	ε ($M^{-1}cm^{-1}$)	Φ
C47	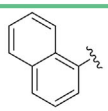	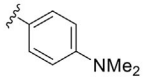	2.42 ± 0.04	411	571	24000	0.02
C48	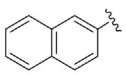	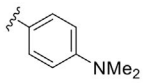	24.08 ± 0.13	433	564	33000	0.16
C49		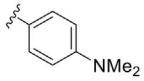	>60	409	511	35400	0.34
C50		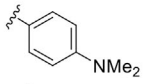	>60	430	556	36800	0.18
C51	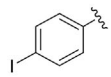	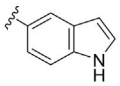	49.55 ± 1.31	367	463	24900	<0.01
C52	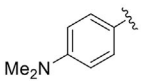	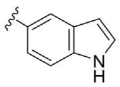	>60	388	412	35700	<0.01
C53	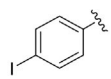	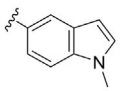	44.34 ± 4.04	372	533	18900	0.01
C54	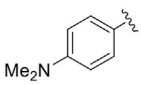	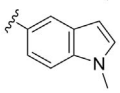	>60	390	/[a]	35700	0
C55	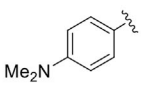	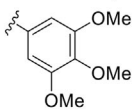	>60	388	/[a]	26000	0
C56	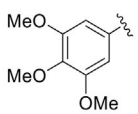	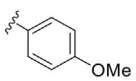	0.77 ± 0.08	347	698	25500	<0.01

[a] No detectable emission under the experimental conditions.

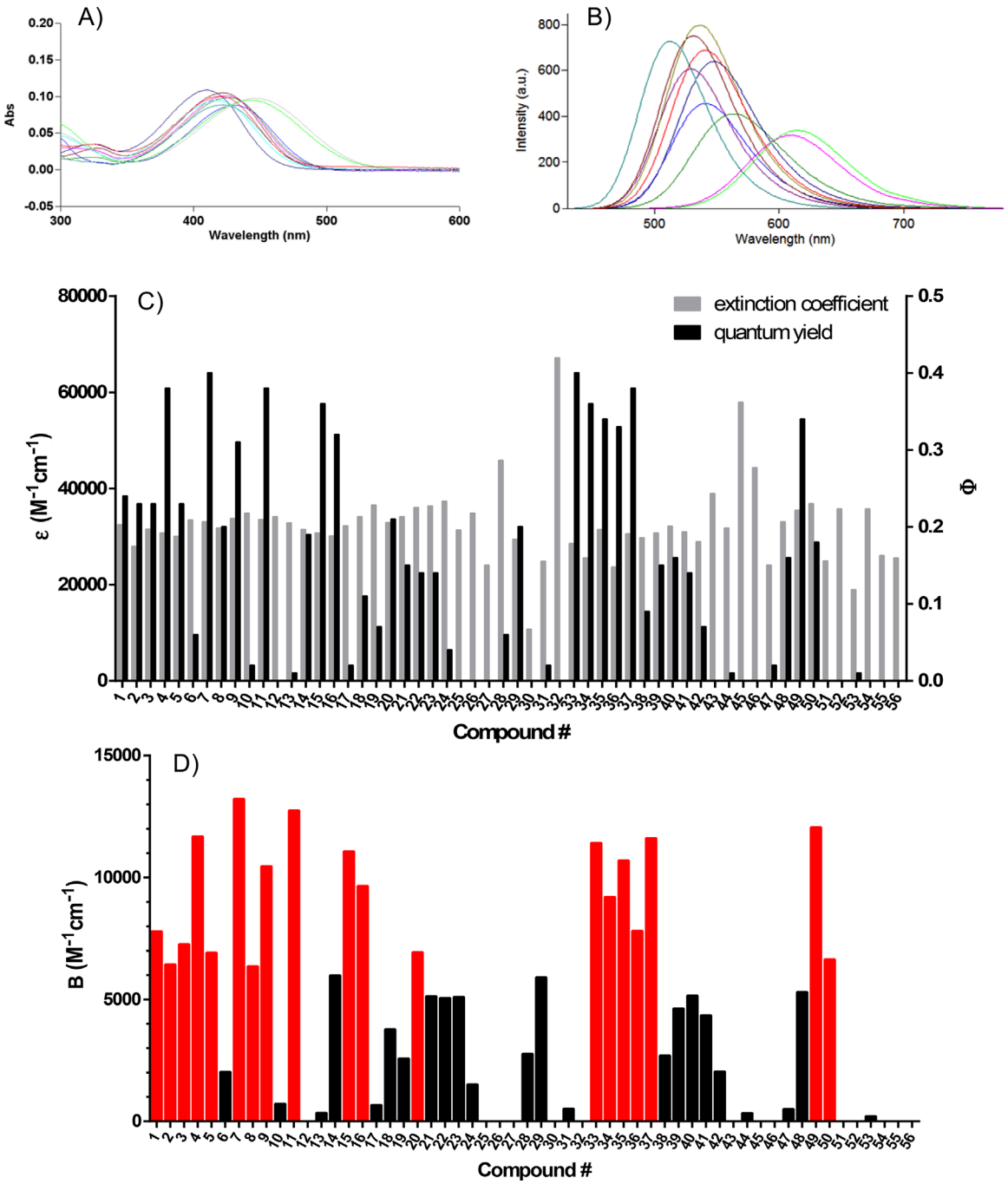

Figure 2. The fluorescence properties of 56 chalcone compounds. (A) The absorption and (B) emission spectra of representative chalcones. (C) The extinction coefficient (ε) and the quantum yield (Φ), and (D) the brightness (compounds with brightness $>6000\,M^{-1}\,cm^{-1}$ highlighted in red).

feature (**C55**, **C56**) were non-fluorescent. Second, the planar conformation of chalcone's core structure, encompassing both rings and the propenone bridge, is important for optimal fluorescence, because compounds with steric hindrance that disfavors such a planar conformation (**C6**, **C10**, **C12**, and **C30**–**C32**) all showed significant decreases in quantum yield. Third, electron donating/withdrawing properties of the substituents on the A ring greatly influence the quantum yield. Weak electron-donating substituents were preferred (**C4**, **C7**, and **C11**, relative to **C1**), while either

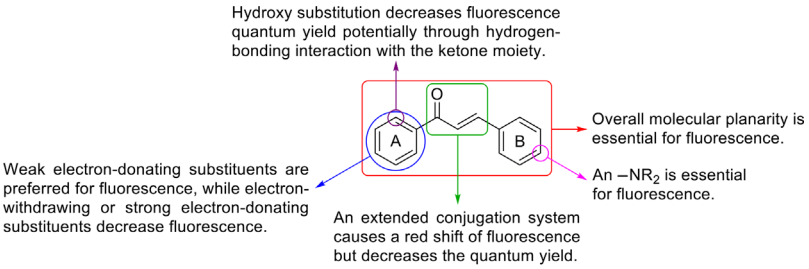

Figure 3. Structural effects on chalcones' fluorescence.

electron withdrawing (**C17**, **C25**–**C27**, relative to **C1**) or strong electron donating substituents (**C28** relative to **C1**) significantly decreased the quantum yield. Fourth, an internal hydrogen bonding interaction with chalcone's ketone moiety (**C13** relative to **C1**) decreased the quantum yield. Lastly, an extended conjugation system (**C38**–**C44**) resulted in a red shift of the maximum emission wavelength and a decrease in quantum yield.

Non-structural factors affecting chalcones' fluorescence

Since the fluorescence of many fluorophores are highly sensitive to their environment [28], the influence of biologically relevant factors, such as solvent, pH, and common biological components, should be characterized in developing biologically useful fluorophores. Compound **C9** was chosen as the model compound to characterize such effects. We first evaluated the solvent effect and observed an overall positive correlation between solvent polarity and fluorescence quantum yield, with the exception of ethanol and water (Fig. 4A). Compound **C9** showed no fluorescence in ethanol or water despite their high polarity. This lack of fluorescence is potentially due to the hydrogen bond formation between the solvent and the basic nitrogen atom of the dialkylamino group on chalcone's B ring [37]. With such an interaction, the nitrogen lone pair electrons cannot delocalize into the conjugation system, which is essential for chalcones' fluorescence [29]. Given the importance of water in all biological systems, we characterized the effect of the amount of water on **C9**'s fluorescence in DMSO. A sharp decrease in fluorescence was observed with increasing percentage of water; and near-complete quenching occurred with >50% water (Fig. 4B). Nevertheless, such an effect could be partially reversed with low concentrations of additives, such as BSA (Fig. 4C), Triton-X100, and Tween-20 (not shown). The quantum yields of **C9** under these conditions were 0.12 with 0.2% BSA, 0.12 with 0.1% Triton-X100, and 0.11 with 0.1% Tween-20. Such a fluorescence recovery is potentially due to the formation of local hydrophobic environments by the additives. The hydrophobic environment may sequester **C9**, making the dialkylamino nitrogen less available for hydrogen-bonding interaction with water. We next evaluated the effect of pH on **C9**'s fluorescence in aqueous solutions with 0.1% Triton-X100 as the additive. The fluorescence intensity remained decently constant within the biological pH range (pH 5–9) but decreased significantly when pH was lower than 3 (Fig. 4D). This may be due to the protonation of the dialkylamino nitrogen under low pH conditions. Lastly, since chalcones are well-known electrophiles to react with biological thiols via Michael addition [40], we tested the effect of such a reaction on **C9**'s fluorescence. Using *N*-acetylcysteamine as the model thiol as previously described [41], we monitored the extent of Michael addition reaction by ^{1}H NMR as the ratio of **C9** to its thiol adduct, with the corresponding fluorescence change measured. The same extent of Michael addition and fluorescence reduction was observed (Fig. 4E), indicating that the thiol adduct was essentially non-fluorescent. This suggests that chalcone-based fluorescent probes would lose their fluorescence if the mechanism of action involves covalent modification of the cellular target via Michael addition.

Cytotoxicity and a sharp SAR

We next explored the potential of fluorescent chalcones as probes for mechanistic investigation. Among the reported bioactivities, cytotoxicity was selected because chalcones' cytotoxicity is highly sensitive to the structure, indicating a well-defined binding interaction with the responsible target [42, 43]. We determined the cytotoxicity of our chalcone compounds against A549, a human non-small cell lung adenocarcinoma cell line (Table 1). As expected, these compounds exhibited a wide range of cytotoxicity, with IC_{50} values (the concentration to inhibit A549 cell proliferation by 50%) varying from high nanomolar (**C2**, $IC_{50} = 250$ nM) to high micromolar ($IC_{50} > 60\ \mu$M). Moreover, the cytotoxicity is highly sensitive to even subtle structural changes, especially at the A ring (Fig. 5). First, compounds with any *para*-substitution on the A ring showed decreased potency than their unsubstituted counterparts (**C4**, **C15**, **C17**, **C20**–**C23**, and **C27**–**C29** compared to **C1**; **C5** compared to **C2**; **C7** compared to **C3**; and **C9** compared to **C8**). These results suggest that the binding pocket for the A ring has limited space to accommodate *para*-substitution. Second, any substituent, other than a hydroxyl, on the *ortho* position of the A ring improved the potency (**C2**, **C14**, **C24**, and **C25** compared to **C1**). However, if both *ortho* positions were substituted, the potency was lost (**C6**, **C10**, and **C12**). Third, a methoxy substitution at the

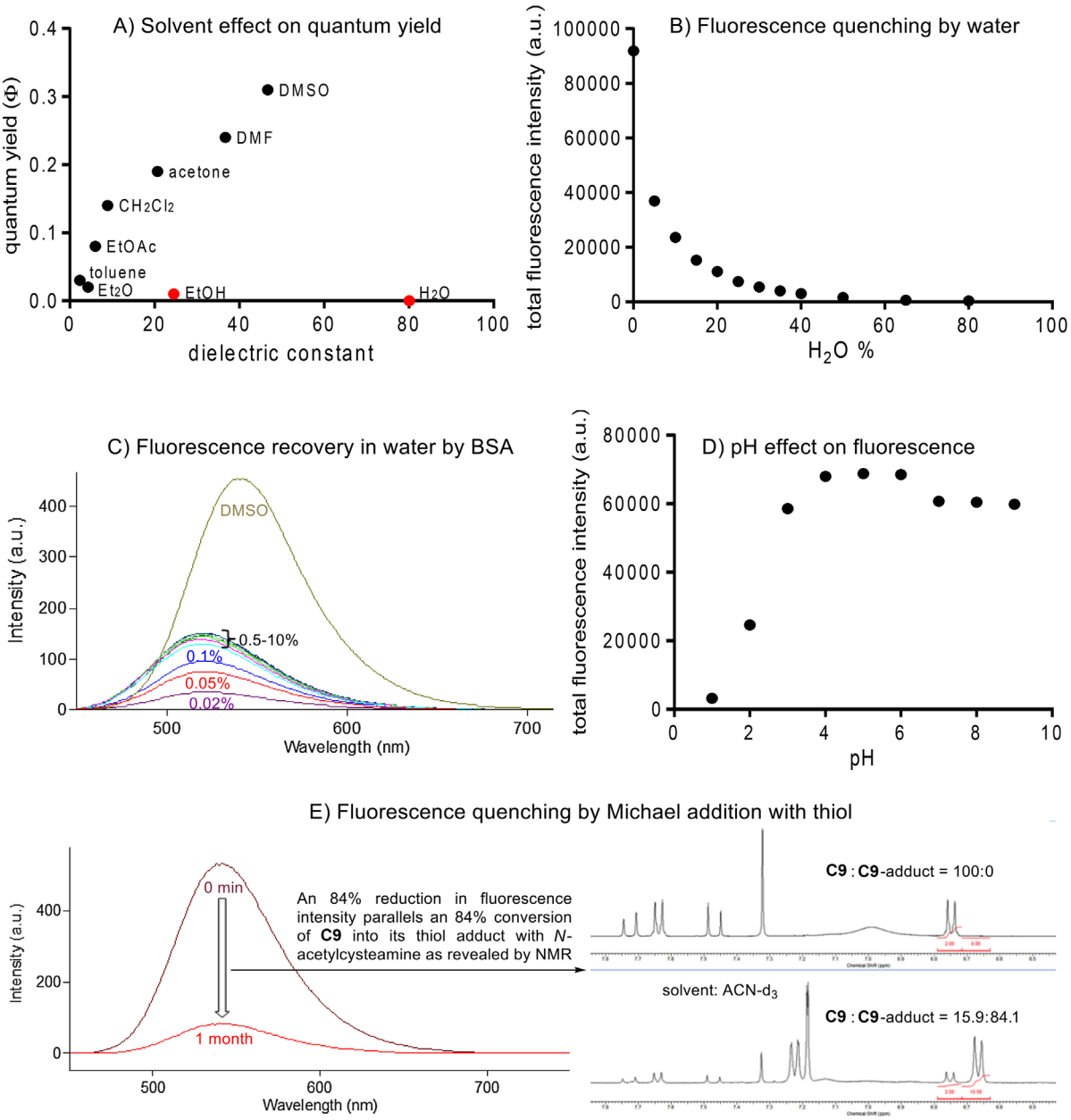

Figure 4. Non-structural factors that influence **C9**'s fluorescence properties. (A) The quantum yield of **C9** in different solvents. (B) The effect of different percentage of water on **C9**'s fluorescence in DMSO. (C) Fluorescence recovery of **C9** by BSA in water. (D) The effect of pH on **C9**'s fluorescence. (E) The effect of thiol adduct formation on **C9**'s fluorescence.

meta-substituent improved potency (**C3** compared to **C1**; **C7** compared to **C4**), and substitution of both *meta* positions with methoxy or methyl was further preferred (**C8**, **C9**, and **C16**). Fourth, the dimethylamino group on the *para* position of the B ring was not essential for cytotoxicity, as other dialkylamino groups (**C33**, **C34**, and **C37**) or methoxy group (**C56**) at the same position also gave comparable potency. Fifth, a methyl group on the alkene α-carbon considerably increased the potency (**C30** compared to **C1**), which is consistent with the observations in the literature [11]. Finally, compounds with modified scaffolds, such as the extended chalcones (**C38**–**C44**), the bis-chalcones (**C45**, **C46**), the ring-constrained chalcones (**C31**, **C32**), and the heterocyclic chalcones (**C49**–**C55**), all showed reduced potency relative to their

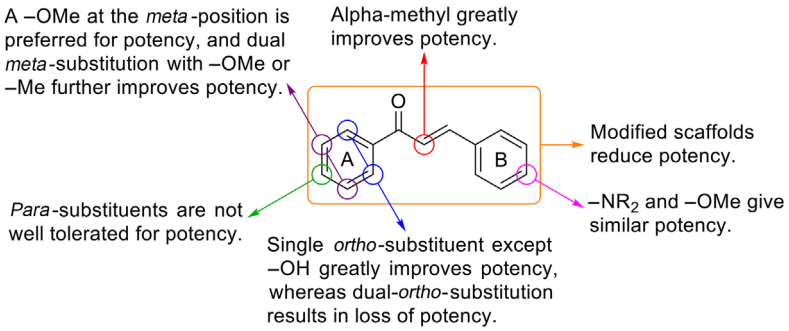

Figure 5. Structure–activity relationship of chalcones' cytotoxicity.

chalcone counterparts. In summary, these chalcones exhibited diverse cytotoxicity potencies with a sharp SAR.

Cell cycle arrest and cellular microtubule depolymerization by cytotoxic chalcones

Since cell cycle arrest has been reported to be involved in chalcones' cytotoxicity [12], we characterized the effect of our cytotoxic chalcones (**C8** and **C16**) on cell cycle distribution in comparison to the non-potent ones (**C4** and **C1**). Cells treated with **C8** and **C16** showed significantly increased population in G2/M phases relative to the control, and the effect was greater with the more potent **C8** (Fig. 6A). The non-cytotoxic compounds **C1** and **C4** showed no effect under the same treatment conditions. The effect of **C8** on cell cycle was dose- and time dependent (Fig. 6B and C). Interestingly, such an

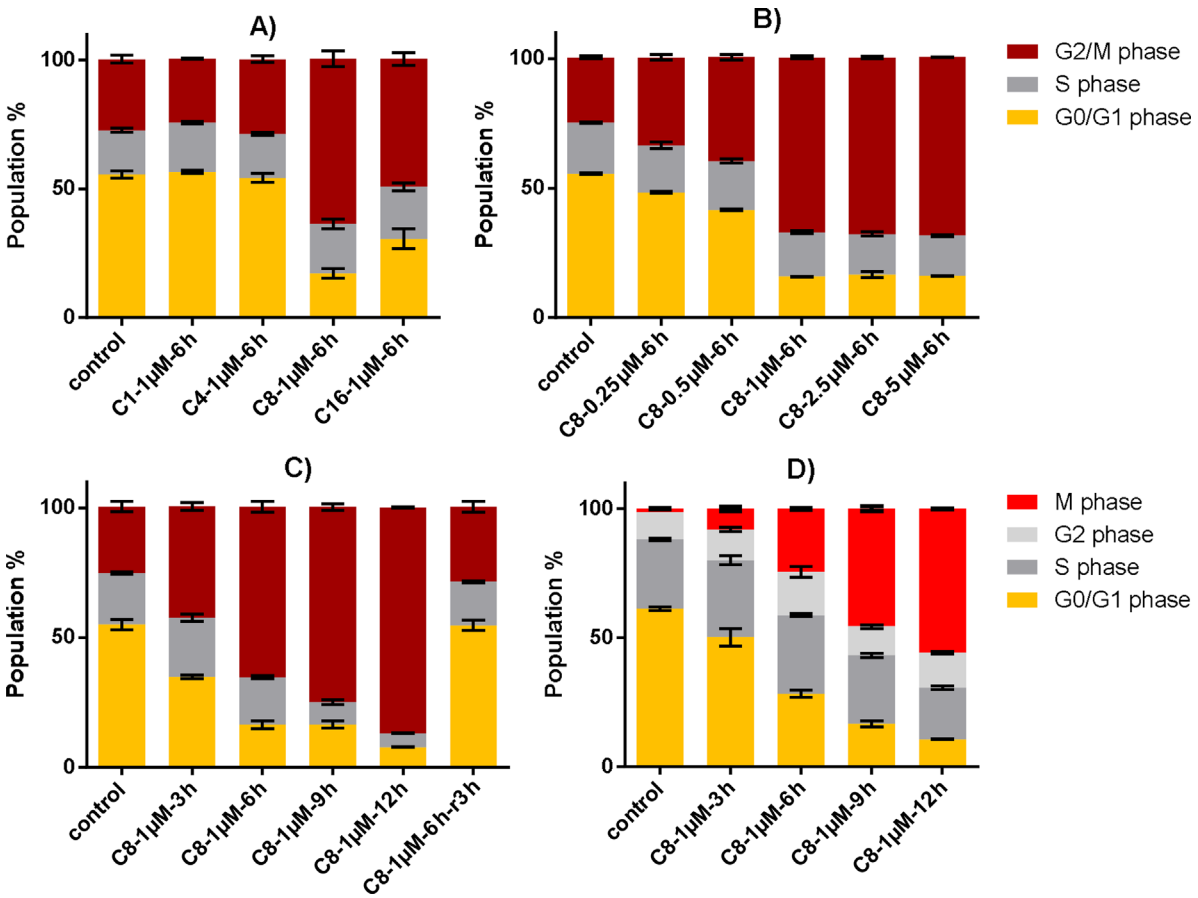

Figure 6. Cell cycle arrest by the cytotoxic chalcones. (A) The effect of different chalcones on the cell cycle at 1 μM for 6 h. (B) The dose response of **C8** on the cell cycle at 6 h. (C) The time dependence of the cell cycle effect of **C8** at 1 μM (the treatment regimen for the last bar was **C8** at 1 μM for 6 h followed by treatment removal for 3 h). (D) **C8** arrested cells at the M phase, not the G2 phase.

effect was readily reversible, as cells re-distributed to the normal cell cycle population upon **C8** removal (last bar in Fig. 6C), suggesting a non-covalent interaction of **C8** with its responsible cellular target for cytotoxicity. This suggests that **C8**'s fluorescence would likely be retained upon target interaction. Finally, **C8** time dependently arrested the cells in the M phase (Fig. 6D).

We next investigated the effect of these four chalcones on microtubule structure in A549 cells since chalcone-based compounds have been suggested to disrupt cellular microtubule structure, leading to cell cycle arrest [12]. A549 cells were treated with **C1**, **C4**, **C8**, and **C16**, and the microtubule structure was visualized via anti-tubulin immunostaining as previously described [12]. As expected, non-cytotoxic **C1** and **C4** had no obvious effect on the microtubule structure in comparison to the control cells (Fig. 7). A significant decrease of the microtubule structure was observed in cells treated with the cytotoxic **C8** and **C16**. The extent of decrease was higher in **C8**-treated cells relative to **C16**-treated samples, consistent with the higher potency of **C8** relative to **C16**.

These results overall strongly support that M-phase cell cycle arrest caused by cellular microtubule depolymerization is likely involved in the mechanism of chalcones' cytotoxicity.

Confocal microscopy of cytotoxic probe C8 for cellular distribution and its potential interaction with tubulin

Since many tubulin-interacting agents have shown similar cell cycle arrest and microtubule depolymerization effect [44], we speculated that the cytotoxic chalcones would interact with tubulin in cells. This was tested via the confocal microscopy imaging taking advantage of chalcones' intrinsic fluorescence. Fluorescent cytotoxic **C8** was selected as the probe. Pre-fixed and permeabilized A549 cells were stained with fluorescently labeled β-tubulin antibody and then treated with **C8**. Fluorescence images were taken with a green channel for **C8** and a red channel for tubulin. Under the experimental conditions, **C8** unexpectedly showed widespread fluorescence in the cytosol with significant bright spots not corresponding to the tubulin network (Fig. 8). These bright spots overall do not have well-defined structures, suggesting potential precipitation of **C8**. Nevertheless, a closer inspection revealed weak but discernible co-localization of **C8** with tubulin at the mitotic spindles, where tubulin was highly concentrated (Fig. 8). Further attempts to reduce the bright spots by decreasing **C8** concentration did

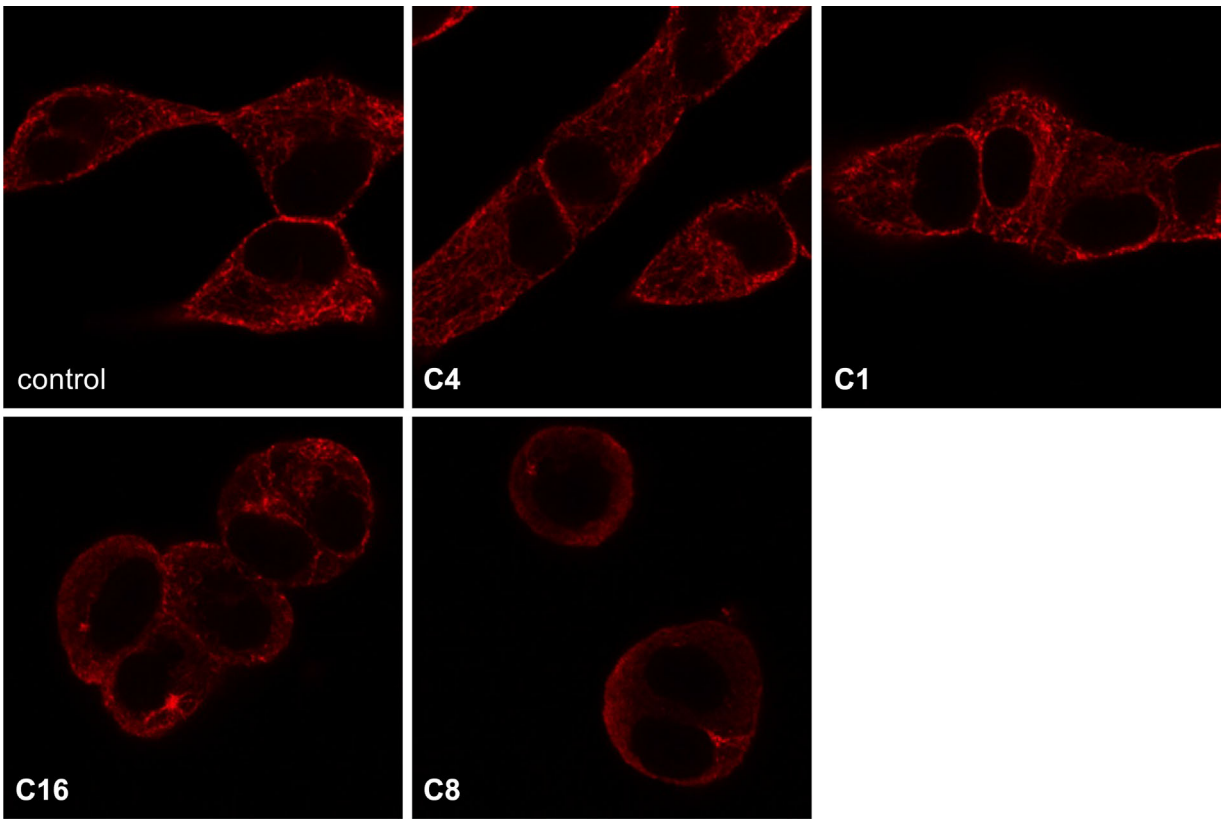

Figure 7. The effect of different chalcone compounds on cellular microtubule structures in A549 cells via immunofluorescence microscopy (magnification: 1000×).

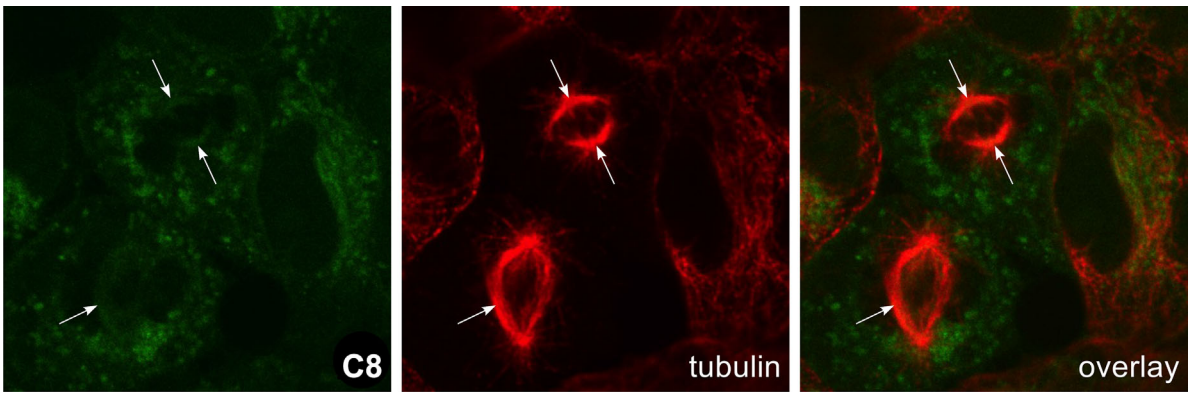

Figure 8. Co-localization of **C8** with tubulin at mitotic spindles in A549 cells via confocal microscopy (magnification: 1000×). Green channel: **C8** fluorescence; red channel: anti-tubulin fluorescence. White arrows indicate the mitotic spindle structures where weak but discernible co-localization of **C8** and tubulin.

not result in better images (data not shown). Given the high sensitivity of chalcones' fluorescence to environmental factors, the non-optimal pattern may not accurately reflect the extent and specificity of biological interactions. Nevertheless, the weak co-localization signal in the cells did provide supporting evidence of direct cellular interaction of cytotoxic chalcones with tubulin.

Conclusion

In summary, we have investigated the influence of structural and environmental factors on chalcones' intrinsic fluorescence, and explored their potential as chemical probes in mechanistic investigations. Important structural effects were observed with chalcones' fluorescence properties. The 4-dialkylamino group on the B ring and the overall planar conformation are essential for optimal fluorescence, while the electronic properties of the substituents on the A ring affect the quantum yield. With respect to environmental factors, water quenches chalcones' fluorescence, which can be partially reversed by the addition of a minimal amount of biologically friendly additives. Based on this observation, the fluorescence in detected cells may derive from chalcone's binding to its cellular target(s) while the free form would have minimal fluorescence, which can be of great benefit to target identification. Finally, chalcones' fluorescence would disappear upon covalent modification by thiols via Michael addition. This property is interesting as well for target/mechanistic investigation. For instance, we have observed the co-localization of **C8** with tubulin via fluorescence, which suggests that such an interaction is not mediated via covalent modification, consistent with the reversibility of the cell cycle arrest effect.

For chalcones' cytotoxicity, a *para*-substitution on the A ring decreases potency while an *ortho*-substitution on the A ring, a single or dual *meta*-methoxylation, or an α-methylation increases the potency. The extent of cell cycle arrest and cellular microtubule depolymerization correlated nicely with the cytotoxic potency of chalcones, supporting the anti-microtubule mechanism of action. Results from confocal microscopy studies provided novel evidence suggesting that cytotoxic chalcones physically interact with tubulin in cells.

The high sensitivity of chalcones' fluorescence properties to environmental factors presents both an opportunity and a challenge. The results revealed herein provide guidance for the future development of fluorescent chalcone probes, particularly for applications with simple scenarios, such as certain cell type staining and Aβ plaque imaging [29, 30].

Experimental

Chemistry

Chemicals and reagents

All reagents and solvents were purchased from vendors and used without further purification. Column chromatography was performed on Whatman silica gel 60 Å (230–400 mesh). NMR (^{1}H and ^{13}C) spectra were recorded on a Bruker spectrometer and calibrated using the deuterated solvent residual as an internal reference. ESI positive mode mass spectra were recorded on an Agilent MSD SL ion trap. HPLC purity of the compounds was analyzed using a C18 column with a gradient acetonitrile/water elution from 30 to 70% acetonitrile over a period of 45 min at a flow rate of 0.5 mL min^{-1}.

The InChI codes of the investigated compounds are provided in the Supporting Information.

Synthesis of chalcones

To a stirred solution of the corresponding acetophenone (3.33 mmol, 1.0 eq.) and the corresponding benzaldehyde

(3.67 mmol, 1.1 eq.) dissolved in EtOH (10 mL) was added sodium hydroxide (10 mmol, 3.0 eq.). This mixture was stirred under room temperature (or at 50°C for slow reactions) for 6–12 h. A yellow precipitate typically formed. Crude product was collected via filtration followed by recrystallization in cold MeOH to yield the pure product as a colored crystalline solid. For products that did not precipitate, ethyl acetate/H_2O extraction followed by chromatography of the organic residue was performed to purify the product with ethyl acetate/hexanes as the eluents. Purities of all compounds were >95% based on HPLC analysis. For known compounds, ^{1}H NMR spectra were compared with literature reports and found to be consistent. NMR and MS characterization of all new compounds are reported below.

*(E)-1-(3,5-Dimethoxyphenyl)-3-(4-(dimethylamino)phenyl)-prop-2-en-1-one (**C8**)*
Yield: 75%; ^{1}H NMR (400 MHz, $CDCl_3$): δ 7.79 (1H, d, J = 15.6 Hz), 7.54 (2H, d, J = 8.8 Hz), 7.27 (1H, d, J = 15.6 Hz), 7.14 (2H, d, J = 2.2 Hz), 6.68 (2H, d, J = 8.8 Hz), 6.64 (1H, t, J = 2.2 Hz), 3.86 (6H, s), 3.03 (6H, s); ^{13}C NMR (100 MHz, $CDCl_3$): δ 190.16, 160.73, 152.02, 145.92, 141.12, 130.39, 122.54, 116.82, 111.76, 106.11, 104.40, 55.55, 40.06; MS (ESI, positive) calculated *m/z* for $[M+H]^+$: 312.2; found: 312.1.

*(E)-3-(4-(Dimethylamino)phenyl)-1-(o-tolyl)prop-2-en-1-one (**C14**)*
Yield: 70%; ^{1}H NMR (400 MHz, $CDCl_3$): δ 7.44 (2H, d, J = 9.0 Hz), 7.43 (1H, d, J = 6.8 Hz), 7.37 (1H, d, J = 16.0 Hz), 7.35 (1H, t, J = 7.2 Hz), 7.26 (1H, d, J = 7.2 Hz), 7.25 (1H, t, J = 6.8 Hz), 6.91 (1H, d, J = 16.0 Hz), 6.67 (2H, d, J = 9.0 Hz), 3.03 (6H, s), 2.42 (3H, s); ^{13}C NMR (100 MHz, $CDCl_3$): δ 197.39, 152.22, 147.43, 140.22, 136.44, 131.12, 130.48, 129.86, 127.88, 125.45, 122.35, 122.17, 111.94, 40.23, 20.14; MS (ESI, positive) calculated *m/z* for $[M+H]^+$: 266.2; found: 266.2.

*(E)-3-(4-(Dimethylamino)phenyl)-1-(3,5-dimethylphenyl)-prop-2-en-1-one (**C16**)*
Yield: 74%; ^{1}H NMR (400 MHz, $CDCl_3$): δ 7.78 (1H, d, J = 15.6 Hz), 7.61 (2H, s), 7.56 (2H, d, J = 9.0 Hz), 7.32 (1H, d, J = 15.6 Hz), 7.19 (1H, s), 6.69 (2H, d, J = 9.0 Hz), 3.04 (6H, s), 2.40 (6H, s); ^{13}C NMR (100 MHz, $CDCl_3$): δ 190.99, 151.93, 145.41, 139.14, 137.99, 133.78, 130.31, 126.05, 122.71, 117.25, 111.77, 40.07, 21.26; MS (ESI, positive) calculated *m/z* for $[M+H]^+$: 280.2; found: 280.1.

*(E)-3-(4-(Dimethylamino)phenyl)-1-(4-(trifluoromethyl)-phenyl)prop-2-en-1-one (**C17**)*
Yield: 81%; ^{1}H NMR (400 MHz, $CDCl_3$): δ 8.07 (2H, d, J = 8.2 Hz), 7.80 (2H, d, J = 15.6 Hz), 7.74 (2H, d, J = 8.2 Hz), 7.55 (2H, d, J = 8.8 Hz), 7.27 (1H, d, J = 8.2 Hz), 6.69 (2H, d, J = 8.8 Hz), 3.05 (6H, s), 2.40 (6H, s); ^{13}C NMR (125 MHz, $CDCl_3$): δ 189.71, 152.42, 147.24, 142.19, 133.44 (q, J = 32.3 Hz), 130.82, 128.66, 125.56 (q, J = 3.8 Hz), 123.93 (q, J = 271.0 Hz) 122.32, 116.33, 111.91, 40.18; MS (ESI, positive) calculated *m/z* for $[M+H]^+$: 319.1; found: 319.1.

*(E)-3-(4-(Dimethylamino)phenyl)-1-(4-ethoxy-2,5-difluorophenyl)prop-2-en-1-one (**C18**)*
Yield: 68%; ^{1}H NMR (400 MHz, $CDCl_3$): δ 7.77 (1H, dd, J = 15.6, 2.0 Hz), 7.64 (1H, dd, J = 11.6, 6.8 Hz), 7.52 (2H, d, J = 8.8 Hz), 7.24 (1H, dd, J = 15.6, 2.4 Hz), 6.69 (1H, dd, J = 12.0, 6.8 Hz), 6.67 (2H, d, J = 8.8 Hz), 4.14 (2H, q, J = 6.8 Hz), 3.03 (6H, s), 1.49 (3H, t, J = 6.8 Hz); ^{13}C NMR (125 MHz, $CDCl_3$): δ 186.03 (d, J = 4.3 Hz), 158.12 (dd, J = 249.0, 1.5 Hz), 152.21, 151.17 (dd, J = 12.6, 11 Hz), 148.74 (dd, J = 242.3, 2.2 Hz), 145.78, 130.69, 122.62, 119.97 (d, J = 9.0 Hz), 119.27 (dd, J = 15.2, 4.7 Hz), 117.25 (dd, J = 21.2, 4.9 Hz), 111.89, 102.25 (dd, J = 30.0, 1.3 Hz), 65.43, 40.19, 14.57; MS (ESI, positive) calculated *m/z* for $[M+H]^+$: 332.1; found: 332.1.

*(E)-3-(4-((2-Hydroxyethyl)(methyl)amino)phenyl)-1-(3,4,5-trimethoxyphenyl)prop-2-en-1-one (**C34**)*
Yield: 59%; ^{1}H NMR (500 MHz, $CDCl_3$): δ 7.76 (1H, d, J = 15.5 Hz), 7.52 (2H, d, J = 9.0 Hz), 7.26 (1H, d, J = 15.5 Hz), 7.25 (2H, s), 6.74 (2H, d, J = 9.0 Hz), 3.93 (6H, s), 3.92 (3H, s), 3.84 (2H, t, J = 5.5 Hz), 3.56 (2H, t, J = 5.5 Hz), 3.05 (3H, s), 2.08 (1H, bs); ^{13}C NMR (125 MHz, $CDCl_3$): δ 189.59, 153.14, 151.56, 145.77, 142.05, 134.45, 130.63, 123.05, 116.77, 112.12, 105.99, 61.07, 60.24, 56.47, 54.66, 39.06; MS (ESI, positive) calculated *m/z* for $[M+H]^+$: 372.2; found: 372.2.

*(E)-3-(4-(Pyrrolidin-1-yl)phenyl)-1-(3,4,5-trimethoxyphenyl)-prop-2-en-1-one (**C35**)*
Yield: 72%; ^{1}H NMR (500 MHz, $CDCl_3$): δ 7.80 (1H, d, J = 15.5 Hz), 7.54 (2H, d, J = 8.5 Hz), 7.26 (1H, d, J = 15.5 Hz), 7.26 (2H, s), 6.55 (2H, d, J = 8.5 Hz), 3.94 (6H, s), 3.92 (3H, s), 3.39–3.30 (4H, m), 2.07–1.98 (4H, m). ^{13}C NMR (125 MHz, $CDCl_3$): δ 189.45, 153.12, 149.73, 146.23, 141.90, 134.70, 130.73, 122.13, 115.91, 111.86, 105.91, 61.05, 56.45, 47.70, 25.54; MS (ESI, positive) calculated *m/z* for $[M+H]^+$: 368.2; found: 368.2.

*(2E,4E)-5-(4-(Dimethylamino)phenyl)-1-(2-methoxyphenyl)-penta-2,4-dien-1-one (**C38**)*
Yield: 75%; ^{1}H NMR (400 MHz, $CDCl_3$): δ 7.55 (1H, dd, J = 7.6, 2.0 Hz), 7.46–7.34 (4H, m), 7.01 (1H, td, J = 7.4, 1.0 Hz), 6.97 (1H, d, J = 7.6 Hz), 6.88 (1H, d, J = 15.2 Hz), 6.80 (1H, dd, J = 15.2, 11.2 Hz), 6.78 (1H, d, J = 15.2 Hz), 6.67 (2H, d, J = 8.4 Hz), 3.89 (3H, s), 3.00 (6H, s); ^{13}C NMR (125 MHz, $CDCl_3$): δ 193.43, 157.85, 151.09, 145.64, 142.50, 132.26, 130.12, 129.90, 128.90, 128.02, 124.41, 122.74, 120.66, 112.12, 111.64, 55.80, 40.30; MS (ESI, positive) calculated *m/z* for $[M+H]^+$: 308.2; found: 308.1.

*(2E,4E)-5-(4-(Dimethylamino)phenyl)-1-(3-methoxyphenyl)-penta-2,4-dien-1-one (**C39**)*
Yield: 75%; ^{1}H NMR (400 MHz, $CDCl_3$): δ 7.63 (1H, dd, J = 14.8, 10.8 Hz), 7.55 (1H, d, J = 7.6), 7.52 (1H, d, J = 2.4 Hz), 7.40 (2H, d, J = 8.8 Hz), 7.10 (1H, dd, J = 8.0, 1.2 Hz), 7.00–6.93 (2H, m), 6.85 (1H, dd, J = 14.8, 10.8 Hz), 6.68 (2H, d, J = 8.8 Hz), 3.87 (3H, s), 3.01 (6H, s); ^{13}C NMR (100 MHz, $CDCl_3$): δ 190.33, 159.91, 151.23, 146.54, 143.28, 140.27, 129.52, 129.04, 124.30, 122.78,

122.56, 120.94, 118.99, 112.70, 112.13, 55.56, 40.31; MS (ESI, positive) calculated *m/z* for $[M+H]^+$: 308.2; found: 308.2.

*(2E,4E)-5-(4-(Dimethylamino)phenyl)-1-(3,5-dimethylphenyl)-penta-2,4-dien-1-one (**C41**)*
Yield: 71%; ^{1}H NMR (400 MHz, $CDCl_3$): δ 7.61 (1H, dd, J = 15.2, 11.0 Hz), 7.58 (2H, s), 7.40 (2H, d, J = 8.8 Hz), 7.18 (1H, s), 6.98 (1H, d, J = 15.2 Hz), 6.95 (1H, d, J = 15.2 Hz), 6.85 (1H, dd, J = 15.2, 11.0 Hz), 6.68 (2H, d, J = 8.8 Hz), 3.01 (6H, s), 2.39 (6H, s); ^{13}C NMR (100 MHz, $CDCl_3$): δ 190.99, 151.16, 146.08, 142.91, 138.95, 138.17, 134.05, 128.96, 126.20, 124.39, 123.16, 122.66, 112.15, 40.31, 21.41; MS (ESI, positive) calculated *m/z* for $[M+H]^+$: 306.2; found: 306.2.

*(2E,4E)-5-(4-(Dimethylamino)phenyl)-1-(2-methylphenyl)-penta-2,4-dien-1-one (**C42**)*
Yield: 71%; ^{1}H NMR (400 MHz, $CDCl_3$): δ 7.45–7.30 (4H, m), 7.27–7.17 (3H, m), 7.40 (2H, d, J = 8.8 Hz), 6.85 (1H, d, J = 15.2 Hz), 6.79 (1H, dd, J = 15.2, 9.6 Hz), 6.67 (2H, d, J = 8.4 Hz), 6.55 (1H, d, J = 15.2 Hz), 3.01 (6H, s), 2.42 (3H, s); ^{13}C NMR (100 MHz, $CDCl_3$): δ 197.21, 151.21, 147.92, 143.07, 139.88, 136.53, 131.16, 129.98, 129.06, 127.88, 127.70, 125.45, 124.18, 122.33, 112.15, 40.33, 20.17; MS (ESI, positive) calculated *m/z* for $[M+H]^+$: 292.2; found: 292.1.

*(2E,4E)-5-(4-(Dimethylamino)phenyl)-1-(2-nitrophenyl)-penta-2,4-dien-1-one (**C43**)*
Yield: 79%; ^{1}H NMR (500 MHz, $CDCl_3$): δ 8.12 (1H, dd, J = 8.0, 1.0 Hz), 7.72 (1H, td, J = 7.5, 1.0 Hz), 7.60 (1H, ddd, J = 8.0, 7.5, 1.5 Hz), 7.47 (1H, dd, J = 7.5, 1.0 Hz), 7.34 (2H, d, J = 8.8 Hz), 7.03 (1H, dd, J = 15.0, 10.0 Hz), 6.80 (1H, d, J = 15.0 Hz), 6.74 (1H, dd, J = 15.5, 10.0 Hz), 6.64 (2H, d, J = 8.8 Hz), 6.45 (1H, d, J = 15.5 Hz), 3.00 (6H, s); ^{13}C NMR (125 MHz, $CDCl_3$): δ 192.88, 151.40, 148.35, 146.95, 144.08, 136.91, 133.87, 130.27, 129.27, 129.01, 126.52, 124.53, 123.81, 121.75, 112.05, 40.25; MS (ESI, positive) calculated *m/z* for $[M+H]^+$: 323.1; found: 323.1.

*(2E,2′E)-1,1′-(1,3-Phenylene)bis(3-(4-(dimethylamino)-phenyl)prop-2-en-1-one) (**C45**)*
Yield: 71%; ^{1}H NMR (400 MHz, $CDCl_3$): δ 8.61 (1H, t, J = 1.6 Hz), 8.18 (2H, dd, J = 7.6, 1.6 Hz), 7.84 (2H, d, J = 15.6 Hz), 7.61 (1H, t, J = 7.6 Hz), 7.58 (4H, d, J = 8.8 Hz), 7.39 (2H, d, J = 15.6 Hz), 6.70 (4H, d, J = 8.8 Hz), 3.01 (6H, s), 2.42 (3H, s); ^{13}C NMR (100 MHz, $CDCl_3$): δ 190.10, 152.31, 146.62, 139.40, 131.88, 130.78, 128.85, 128.07, 122.63, 116.62, 111.95, 40.26; MS (ESI, positive) calculated *m/z* for $[M+H]^+$: 425.2; found: 425.2.

Fluorescence characterization

All optical properties were measured with a Varian Cary Eclipse fluorescence spectrophotometer. Compounds were made into 10–50 mM DMSO stock solutions, which were diluted to 3 μM with DMSO in a 1 cm quartz cuvette for the measurement of the maximum absorption wavelength. The same sample was then excited at the maximum absorption wavelength for the measurement of the maximum emission wavelength. The extinction coefficient was obtained by a linear regression of the absorption measured at 10, 20, and 30 μM in DMSO. The quantum yield was determined following an established procedure using fluorescein ($\Phi = 0.79$) as the standard [45]. Briefly, a linear regression of the total fluorescence emission against absorption at different concentrations was performed, with the absorption not exceeding 0.12. For solvent effect, the DMSO stock solution of **C9** (50 mM) was diluted to 3 μM in different solvents for quantum yield characterization. For pH effect, phosphate solutions at pH 1.0–9.0 containing 0.1% Triton X-100 were prepared by mixing 0.1 M NaH_2PO_4 with 0.1 M Na_2HPO_4 or 1 N HCl if needed to the specific pH, followed by addition of the detergent. The DMSO stock solution of **C9** (50 mM) was diluted to 3 μM in these solutions and the fluorescence was measured.

Fluorescence quenching by *N*-acetylcysteamine

C9 (4.3 mg) was dissolved in 425 μL acetonitrile-d_3. To it, 25 μL phosphate buffer in D_2O at pD 9.2 was added. The reaction started by the addition of *N*-acetylcysteamine (NAC) stock solution in acetonitrile-d_3 (50 μL, 2.5 M). The final concentrations of **C9** and NAC were 25 and 250 mM, respectively. The formation of the thiol adduct was monitored by ^{1}H NMR. The doublets at 6.63–6.71 ppm, the characteristic of the adduct, and the doublets at 6.71–6.79 ppm, the characteristic of unreacted **C9**, were integrated; and their ratio was calculated. One microliter of the mixture was diluted 10000-fold with DMSO for fluorescence measurement at the beginning of the reaction and when it reached equilibrium.

Cytotoxicity assay

A549 cells originally obtained from ATCC were cultured in DMEM medium with 10% FBS, penicillin (100 U mL^{-1}), and streptomycin (100 μg mL^{-1}) at 37°C with 5% CO_2. The *in vitro* cytotoxicity of chalcones was assayed by determining the IC_{50} (the concentration of chalcones to inhibit cell growth by 50%) [43]. Briefly, cells were seeded in a 96-well plate at a density of 3000/well. After attachment, cells were treated media containing the compounds at serial dilutions with 1% DMSO. Cells treated with media containing 1% DMSO served as the control. After a 48-h treatment, the relative cell viability in each well was determined in comparison to that in the control wells using the CellTiter-Blue cell viability assay kit. The IC_{50} of each compound was determined by fitting the relative cell viability to the corresponding drug concentrations by using a sigmoidal dose–response model of varied slope in Prism GraphPad 5.0. The IC_{50}s reported herein are the average of at least three biological replicates.

Analysis of cell cycle distribution by flow cytometry

Cell cycle was analyzed by flow cytometry based on DNA content as previously described [46]. Briefly, A549 cells with specified treatments were trypsinized, washed with PBS, and then suspended in PBS (1 mL). This suspension was added to

70% ethanol (9 mL) and stored at 4°C overnight for fixation. Cell pellets were collected by centrifugation, washed twice with PBS, then re-suspended in propidium iodide (PI) staining solution (50 μg mL^{-1} PI, 200 μg mL^{-1} RNase A, and 0.1% Triton-X 100 in PBS, 1 mL) and incubated at room temperature for 30 min in the dark. DNA content and cell cycle population was then analyzed with a BD FACSCalibur flow cytometry system.

Microtubule structure by immunofluorescence microscopy

A549 cells were seeded in 96-well confocal plates at 6000/well. After attachment, cells were treated with media containing 5 μM chalcone compounds with 1% DMSO for 6 h. Media were removed and cells were washed with PBS twice and treated with 4% PFA fixative at 37°C for 12 min. After three washes with PBS, cells were permeabilized with 0.05% Triton X-100/PBS for 5 min at 37°C, and then blocked with 5% donkey serum/PBS at 37°C for 8 min, followed by incubation with 1:100 sheep anti-tubulin antibody (Cat# ATN02, Cytoskeleton) at 37°C for 15 min. After three PBS washes, cells were then treated with 1:100 APC-conjugated donkey-anti-sheep antibody (Cat# 713-136-147, Jackson ImmunoResearch) at 37°C for 8 min. After two more PBS washes, fluorescence images were taken with a Nikon TE2000 inverted confocal microscope.

C8 and microtubule co-localization by confocal microscopy

A549 cells were seeded in 96-well confocal plates at 6000/well. After attachment, cells were fixed, permeabilized, blocked, and incubated with the primary and secondary antibodies as described above. Finally, cells were exposed to **C8** at 0.25 μM for 3 h at 37°C. The medium was replaced with PBS and confocal images were taken immediately with a Nikon TE2000 inverted confocal microscope.

The authors have declared no conflicts of interest.

References

[1] N. K. Sahu, S. S. Balbhadra, J. Choudhary, D. V. Kohli, *Curr. Med. Chem*. **2012**, *19*, 209–225.
[2] D. I. Batovska, I. T. Todorova, *Curr. Clin. Pharmacol*. **2010**, *5*, 1–29.
[3] C. Karthikeyan, N. S. Moorthy, S. Ramasamy, U. Vanam, E. Manivannan, D. Karunagaran, P. Trivedi, *Recent Pat. Anticancer Drug Discov*. **2015**, *10*, 97–115.
[4] S. N. Bukhari, I. Jantan, M. Jasamai, *Mini Rev. Med. Chem*. **2013**, *13*, 87–94.
[5] B. Evranos-Aksoz, F. K. Onurdag, S. O. Ozgacar, *Z. Naturforsch. C* **2015**, *70*, 183–189.
[6] J. Z. Wu, C. C. Cheng, L. L. Shen, Z. K. Wang, S. B. Wu, W. L. Li, S. H. Chen, R. P. Zhou, P. H. Qiu, *Int. J. Mol. Sci*. **2014**, *15*, 18525–18539.
[7] C. T. Hsieh, T. J. Hsieh, M. El-Shazly, D. W. Chuang, Y. H. Tsai, C. T. Yen, S. F. Wu, Y. C. Wu, F. R. Chang, *Bioorg. Med. Chem. Lett*. **2012**, *22*, 3912–3915.
[8] B. Zhou, C. Xing, *Med. Chem*. **2015**, *5*, 388–404.
[9] A. Boumendjel, X. Ronot, J. Boutonnat, *Curr. Drug Targets* **2009**, *10*, 363–371.
[10] M. L. Go, X. Wu, X. L. Liu, *Curr. Med. Chem*. **2005**, *12*, 481–499.
[11] S. Ducki, R. Forrest, J. A. Hadfield, A. Kendall, N. J. Lawrence, A. T. McGown, D. Rennison, *Bioorg. Med. Chem. Lett*. **1998**, *8*, 1051–1056.
[12] C. Zhu, Y. Zuo, R. Wang, B. Liang, X. Yue, G. Wen, N. Shang, L. Huang, Y. Chen, J. Du, X. Bu, *J. Med. Chem*. **2014**, *57*, 6364–6382.
[13] V. Martel-Frachet, M. Keramidas, A. Nurisso, S. DeBonis, C. Rome, J. L. Coll, A. Boumendjel, D. A. Skoufias, X. Ronot, *Oncotarget* **2015**, *6*, 14669–14686.
[14] P. Lorenzo, R. Alvarez, M. A. Ortiz, S. Alvarez, F. J. Piedrafita, A. R. de Lera, *J. Med. Chem*. **2008**, *51*, 5431–5440.
[15] S. K. Jung, M. H. Lee, Y. Lim do, J. E. Kim, P. Singh, S. Y. Lee, C. H. Jeong, T. G. Lim, H. Chen, Y. I. Chi, J. K. Kundu, N. H. Lee, C. C. Lee, Y. Y. Cho, A. M. Bode, K. W. Lee, Z. Dong, *J. Biol. Chem*. **2014**, *289*, 35839–35848.
[16] C. Limper, Y. Wang, S. Ruhl, Z. Wang, Y. Lou, F. Totzke, M. H. Kubbutat, Y. Chovolou, P. Proksch, W. Watjen, *J. Pharm. Pharmacol*. **2013**, *65*, 1393–1408.
[17] S. D. Ramalho, A. Bernades, G. Demetrius, C. Noda-Perez, P. C. Vieira, C. Y. Dos Santos, J. A. da Silva, M. O. de Moraes, K. C. Mousinho, *Chem. Biodivers*. **2013**, *10*, 1999–2006.
[18] Y. Na, J. M. Nam, *Bioorg. Med. Chem. Lett*. **2011**, *21*, 211–214.
[19] R. Stoll, C. Renner, S. Hansen, S. Palme, C. Klein, A. Belling, W. Zeslawski, M. Kamionka, T. Rehm, P. Muhlhahn, R. Schumacher, F. Hesse, B. Kaluza, W. Voelter, R. A. Engh, T. A. Holak, *Biochemistry* **2001**, *40*, 336–344.
[20] R. Monteiro, A. Faria, I. Azevedo, C. Calhau, *J. Steroid. Biochem. Mol. Biol*. **2007**, *105*, 124–130.
[21] T. Kahyo, S. Ichikawa, T. Hatanaka, M. K. Yamada, M. Setou, *J. Pharmacol. Sci*. **2008**, *108*, 364–371.
[22] B. Orlikova, M. Schnekenburger, M. Zloh, F. Golais, M. Diederich, D. Tasdemir, *Oncol. Rep*. **2012**, *28*, 797–805.
[23] B. Zhang, D. Duan, C. Ge, J. Yao, Y. Liu, X. Li, J. Fang, *J. Med. Chem*. **2015**, *58*, 1795–1805.
[24] J. Zhang, F. J. Ji, Y. Gu, X. Y. Zhang, S. X. Qiao, *Pharmacol. Rep*. **2014**, *66*, 515–519.
[25] J. S. Lee, J. W. Lee, N. Kang, H. H. Ha, Y. T. Chang, *Chem. Rec*. **2015**, *15*, 495–510.

[26] J. Sumranjit, S. J. Chung, *Molecules* **2013**, *18*, 10425–10451.
[27] S. Ziegler, V. Pries, C. Hedberg, H. Waldmann, *Angew. Chem., Int. Ed. Engl*. **2013**, *52*, 2744–2792.
[28] N. Fili, C. P. Toseland, *EXS* **2014**, *105*, 1–24.
[29] S. C. Lee, N. Y. Kang, S. J. Park, S. W. Yun, Y. Chandran, Y. T. Chang, *Chem. Commun. (Cambridge, U. K.)* **2012**, *48*, 6681–6683.
[30] M. Ono, R. Watanabe, H. Kawashima, Y. Cheng, H. Kimura, H. Watanabe, M. Haratake, H. Saji, M. Nakayama, *J. Med. Chem*. **2009**, *52*, 6394–6401.
[31] M. Tomasch, J. S. Schwed, L. Weizel, H. Stark, *Front. Syst. Neurosci*. **2012**, *6*, 14.
[32] M. C. Cui, M. Ono, H. Kimura, B. L. Liu, H. Saji, *Bioorg. Med. Chem. Lett*. **2011**, *21*, 980–982.
[33] M. Gaber, T. A. Fayed, S. A. El-Daly, Y. S. El-Sayed, *Photoch. Photobio. Sci*. **2008**, *7*, 257–262.
[34] T. A. Fayed, M. K. Awad, *Chem. Phys*. **2004**, *303*, 317–326.
[35] V. Gulbinas, G. Kodis, S. Jursenas, L. Valkunas, A. Gruodis, J. C. Mialocq, S. Pommeret, T. Gustavsson, *J. Phys. Chem. A* **1999**, *103*, 3969–3980.
[36] P. F. Wang, S. K. Wu, *J. Photochem. Photobiol. A* **1995**, *86*, 109–113.
[37] C. G. Niu, A. L. Guan, G. M. Zeng, Y. G. Liu, Z. W. Li, *Anal. Chim. Acta* **2006**, *577*, 264–270.
[38] U. Resch-Genger, M. Grabolle, S. Cavaliere-Jaricot, R. Nitschke, T. Nann, *Nat. Methods* **2008**, *5*, 763–775.
[39] C. Wurth, M. Grabolle, J. Pauli, M. Spieles, U. Resch-Genger, *Nat. Protoc*. **2013**, *8*, 1535–1550.
[40] C. Hu, D. Nikolic, A. L. Eggler, A. D. Mesecar, R. B. van Breemen, *Anal. Biochem*. **2012**, *421*, 108–114.
[41] S. Amslinger, N. Al-Rifai, K. Winter, K. Wormann, R. Scholz, P. Baumeister, M. Wild, *Org. Biomol. Chem*. **2013**, *11*, 549–554.
[42] S. Ducki, G. Mackenzie, N. J. Lawrence, J. P. Snyder, *J. Med. Chem*. **2005**, *48*, 457–465.
[43] B. Srinivasan, T. E. Johnson, R. Lad, C. Xing, *J. Med. Chem*. **2009**, *52*, 7228–7235.
[44] B. Gigant, A. Cormier, A. Dorleans, R. B. Ravelli, M. Knossow, *Top. Curr. Chem*. **2009**, *286*, 259–278.
[45] L. S. Matchette, A. Agrawal, T. J. Pfefer, *Photochem. Photobiol*. **2007**, *83*, 1386–1393.
[46] D. Cao, X. Han, G. Wang, Z. Yang, F. Peng, L. Ma, R. Zhang, H. Ye, M. Tang, W. Wu, K. Lei, J. Wen, J. Chen, J. Qiu, X. Liang, Y. Ran, Y. Sang, M. Xiang, A. Peng, L. Chen, *Eur. J. Med. Chem*. **2013**, *62*, 579–589.